A 2.5D BiCGS-FFT Forward Solver to Model Scattering in a mm-Wave Imaging System

S. Van den Bulcke[1], A. Franchois[1], L. Zhang[2] and J. Stiens[2]

[1] Department of Information Technology (INTEC-IMEC), Ghent University, Belgium,
email: sara.vandenbulcke@ugent.be, ann.franchois@ugent.be
[2] ETRO-TW, Vrije Universiteit Brussel (VUB), Belgium, email: lzhang@etro.vub.ac.be, jstiens@etro.vub.ac.be

Abstract

We present an exact forward solver to compute the three-dimensional electric field scattered by a two-dimensional inhomogeneous dielectric object, illuminated with a given three-dimensional time-harmonic field. A volume integral equation approach is used and the resulting contrast source integral equation is discretized with the Method of Moments and solved iteratively with a stabilized biconjugate gradient Fast Fourier Transform method. Simulation results are compared to analytic solutions for TE and TM polarizations and to measurement results, obtained with a free-space active millimeter wave imaging system.

I. Introduction

A free-space active mm-wave imaging system is being developed at the VUB, in order to study the performance of various imaging modes for applications in indoor security and non-destructive testing. The system consists of a mm-wave vector network analyzer operating in the 75 to 300 GHz range, which measures the S-parameters in amplitude and phase with a dynamic range of more than 80 dB. At the transmitting side a horn antenna emits an incident Gaussian beam, which is focused by two parabolic reflectors at the object location. At the receiving side the scattered field is focused by two parabolic reflectors for image formation at a receiving horn antenna. This optical approach is a qualitative technique for image formation. Another imaging mode is a quantitative technique, which is derived from microwave imaging principles and is largely based on the exact solution of Maxwell's equations. In both cases, an exact model of the wave-field propagation and scattering is indispensable to carefully study system performance and imaging capabilities. Therefore we developed an exact forward solver for two-dimensional (2D) inhomogeneous dielectric objects embedded in a homogeneous background medium. The objects are illuminated with a given three-dimensional (3D) time-harmonic incident field and the 3D scattered field is computed. This 2.5D configuration is adopted since it reduces the computational burden while maintaining the capability of accurately studying the system performance. A volume integral equation approach is used, whereby a contrast source integral equation is discretized with the Method of Moments (MoM) and solved iteratively with a stabilized biconjugate gradient Fast Fourier Transform (BiCGS-FFT) method. The formulation of the algorithm is given in section II and comparisons of simulation results to analytic solutions for TE and TM polarizations and to measurements are presented in section III.

II. Formulation

The 2.5D solver presented in this paper is based on the 2D-TE CG-FFT forward solver developed by [1]. We consider a 2D inhomogeneous dielectric object embedded in free space with complex permittivity $\epsilon(\mathbf{r}) = \epsilon_r(\mathbf{r})\epsilon_0 = \epsilon'(\mathbf{r}) + j\epsilon''(\mathbf{r})$, with $\epsilon'(\mathbf{r})$ and $\epsilon''(\mathbf{r})$ representing the real and imaginary part of $\epsilon(\mathbf{r})$ and $\mathbf{r} = (x, y)$ the position vector. The imaginary part of the relative complex permittivity $\epsilon_r(\mathbf{r})$ is given by $\epsilon_r''(\mathbf{r}) = \frac{\sigma}{\omega\epsilon_0}$, with ω the angular frequency, ϵ_0 the permittivity of vacuum and σ the electric conductivity. The object is illuminated with a 3D time-harmonic incident field $\mathbf{E}^i(\mathbf{r}, z) = [E_1^i(\mathbf{r}, z), E_2^i(\mathbf{r}, z), E_3^i(\mathbf{r}, z)]$ and the resulting scattered field is defined as $\mathbf{E}^s(\mathbf{r}, z) = \mathbf{E}(\mathbf{r}, z) - \mathbf{E}^i(\mathbf{r}, z)$ with $\mathbf{E}(\mathbf{r}, z)$ the total field. The time dependence $\exp(-j\omega t)$ is omitted in the following. The problem is formulated in terms of the unknown electric flux density $\mathbf{D}(\mathbf{r}, z) = [D_1(\mathbf{r}, z), D_2(\mathbf{r}, z), D_3(\mathbf{r}, z)]$. When $\mathbf{E}^i(\mathbf{r}, z)$ is expanded as $\mathbf{E}^i(\mathbf{r}, \beta)e^{j\beta z}$, the integral equation over the object domain S takes the following form

$$\begin{bmatrix} E_1^i(\mathbf{r},\beta) \\ E_2^i(\mathbf{r},\beta) \\ E_3^i(\mathbf{r},\beta) \end{bmatrix} = \frac{1}{\epsilon(\mathbf{r})} \begin{bmatrix} D_1(\mathbf{r},\beta) \\ D_2(\mathbf{r},\beta) \\ D_3(\mathbf{r},\beta) \end{bmatrix} - \begin{bmatrix} k_0^2 + \frac{\partial^2}{\partial x^2} & \frac{\partial^2}{\partial x \partial y} & j\beta\frac{\partial}{\partial x} \\ \frac{\partial^2}{\partial x \partial y} & k_0^2 + \frac{\partial^2}{\partial y^2} & j\beta\frac{\partial}{\partial y} \\ j\beta\frac{\partial}{\partial x} & j\beta\frac{\partial}{\partial y} & k_0^2 - \beta^2 \end{bmatrix} \begin{bmatrix} A_1(\mathbf{r},\beta) \\ A_2(\mathbf{r},\beta) \\ A_3(\mathbf{r},\beta) \end{bmatrix}, \quad \mathbf{r} \in S, \tag{1}$$

where $k_0 = \omega\sqrt{\epsilon_0\mu_0}$. The vector potential $\mathbf{A}(\mathbf{r}, \beta)$ can be calculated as

$$\mathbf{A}(\mathbf{r}, \beta) = F^{-1}[F[G(\mathbf{r}, \beta)]\ F[\chi(\mathbf{r})\frac{\mathbf{D}(\mathbf{r}, \beta)}{\epsilon(\mathbf{r})}]] \tag{2}$$

with F the forward 2D spatial Fourier transform and F^{-1} the inverse 2D spatial Fourier transform. The scalar 2D Green's function is given by $G(\mathbf{r}, \beta) = \frac{j}{4}H_0^{(1)}(\sqrt{k_0^2 - \beta^2}|\mathbf{r}|)$ and the normalized contrast function $\chi(\mathbf{r})$ is defined as $\chi(\mathbf{r}) = \frac{\epsilon(\mathbf{r}) - \epsilon_0}{\epsilon(\mathbf{r})}$.

The β-dependence is assumed in the following.
The spatial coordinate $\mathbf{r}$ is discretized by means of a rectangular 2D grid with a cell size of Δ in both directions and with N cells in the x-direction and M cells in the y-direction. We introduce the following staggered grids for $n = 0 \dots N$ and $m = 0 \dots M$: $\mathbf{r}_{n,m}^{(0)} = (n\Delta, m\Delta)$, $\mathbf{r}_{n,m}^{(1)} = ((n-\frac{1}{2})\Delta,\ m\Delta)$, $\mathbf{r}_{n,m}^{(2)} = (n\Delta,\ (m-\frac{1}{2})\Delta)$ and $\mathbf{r}_{n,m}^{(3)} = ((n-\frac{1}{2})\Delta,\ (m-\frac{1}{2})\Delta)$. In each cell with center $\mathbf{r}_{n,m}^{(0)}$ the complex permittivity $\epsilon(\mathbf{r})$ is assumed constant. Vectorial testing functions $\Psi^{(p)}(\mathbf{r}_{n,m}^{(p)} - \mathbf{r}) = \psi^{(p)}(\mathbf{r}_{n,m}^{(p)} - \mathbf{r})\mathbf{u}^{(p)}$ are introduced for $p = 1, 2, 3$. $\mathbf{u}^{(1)}$, $\mathbf{u}^{(2)}$ and $\mathbf{u}^{(3)}$ represent the unit vectors in the x, y and z-direction. Multiplication of (1) with these vectorial testing functions and integration over S yields:

$$\int_S \psi^{(p)}(\mathbf{r}_{n,m}^{(p)} - \mathbf{r}) E_p^i(\mathbf{r}) \mathrm{d}\mathbf{r} = \int_S \psi^{(p)}(\mathbf{r}_{n,m}^{(p)} - \mathbf{r}) \frac{D_p(\mathbf{r})}{\epsilon(\mathbf{r})} \mathrm{d}\mathbf{r} - k_0^2 \int_S \psi^{(p)}(\mathbf{r}_{n,m}^{(p)} - \mathbf{r}) A_p(\mathbf{r}) \mathrm{d}\mathbf{r} + \int_S \partial_p \psi^{(p)}(\mathbf{r}_{n,m}^{(p)} - \mathbf{r}) div\mathbf{A}(\mathbf{r}) \mathrm{d}\mathbf{r},$$
$$\mathbf{r}_{n,m}^{(p)} \in S,\ p = 1, 2 \quad (3a)$$

$$\int_S \psi^{(3)}(\mathbf{r}_{n,m}^{(3)} - \mathbf{r}) E_3^i(\mathbf{r}) \mathrm{d}\mathbf{r} = \int_S \psi^{(3)}(\mathbf{r}_{n,m}^{(3)} - \mathbf{r}) \frac{D_3(\mathbf{r})}{\epsilon(\mathbf{r})} \mathrm{d}\mathbf{r} - k_0^2 \int_S \psi^{(3)}(\mathbf{r}_{n,m}^{(3)} - \mathbf{r}) A_3(\mathbf{r}) \mathrm{d}\mathbf{r} - j\beta \int_S \psi^{(3)}(\mathbf{r}_{n,m}^{(3)} - \mathbf{r}) div\mathbf{A}(\mathbf{r}) \mathrm{d}\mathbf{r},$$
$$\mathbf{r}_{n,m}^{(3)} \in S. \quad (3b)$$

In the derivation of this equations it was assumed that $\psi^{(p)}(\mathbf{r}_{n,m}^{(p)} - \mathbf{r}) = 0$ for $\mathbf{r} \in \partial S$. ∂_1 and ∂_2 represent the partial derivatives with respect to x and y. The Gauss theorem is used for every subdomain where $\psi^{(p)}(\mathbf{r}_{n,m}^{(p)} - \mathbf{r}) div\mathbf{A}$ is continuous differentiable and the continuity of the normal component of $\psi^{(p)}(\mathbf{r}_{n,m}^{(p)} - \mathbf{r}) div\mathbf{A}$ through the interfaces between the subdomains is used. The electric flux density $\mathbf{D}(\mathbf{r})$, the incident field $\mathbf{E}^i(\mathbf{r})$ and the vector potential $\mathbf{A}(\mathbf{r})$ are expanded as:

$$D_p(\mathbf{r}) = \epsilon_0 \sum_{k=1}^{N} \sum_{l=1}^{M} d_{p;k,l}\ \psi^{(p)}(\mathbf{r} - \mathbf{r}_{k,l}^{(p)}), \quad (4a)$$

$$E_p^i(\mathbf{r}) = \sum_{k=1}^{N} \sum_{l=1}^{M} e_{p;k,l}^i\ \psi^{(p)}(\mathbf{r} - \mathbf{r}_{k,l}^{(p)}), \quad (4b)$$

$$A_p(\mathbf{r}) = \sum_{k=1}^{N} \sum_{l=1}^{M} a_{p;k,l}\ \psi^{(p)}(\mathbf{r} - \mathbf{r}_{k,l}^{(p)}). \quad (4c)$$

When inserting (4) in (3) and carrying out the divergence operator as well as interchanging the order of integration and summation, the weak form of the integral equation is obtained for every $\mathbf{r}_{n,m}^{(p)} \in S$ ($p = 1, 2, 3$). The functions $\psi^{(p)}(\mathbf{r})$, $p = 1, 2, 3$ are defined as:

$$\psi^{(1)}(\mathbf{r}) = \Lambda(x; 2\Delta)\Pi(y; \Delta), \quad (5a)$$

$$\psi^{(2)}(\mathbf{r}) = \Pi(x; \Delta)\Lambda(y; 2\Delta), \quad (5b)$$

$$\psi^{(3)}(\mathbf{r}) = \Lambda(x; 2\Delta)\Lambda(y; 2\Delta), \quad (5c)$$

in which $\Lambda(x; 2\Delta)$ represents a one-dimensional triangle function in the x-direction of support 2Δ and $\Pi(y; \Delta)$ represents a one-dimensional pulse function in the y-direction of support Δ.
In (2) the field values of $\mathbf{D}(\mathbf{r})$ are replaced by the discrete values $d_{p;n,m}$ and 2D spatial discrete Fourier transforms are used. Therefore the Green's function is integrated over a circle with center $\mathbf{r}_{n,m}^{(0)}$ and radius $\frac{\Delta}{2}$. The resulting value is then divided by the surface of that circle:

$$g_{n,m} = \begin{cases} (\frac{j}{\Delta k_0}) J_1(k_0 \frac{\Delta}{2}) H_0^{(1)}(k_0 \Delta \sqrt{n^2 + m^2}) \\ (\frac{j}{\Delta k_0}) \left[H_1^{(1)}(k_0 \frac{\Delta}{2}) + \frac{4j}{\pi \Delta k_0} \right] \qquad n = m = 0. \end{cases} \quad (6)$$

This procedure gives no problem in handling the singularity of the Green's function at $\mathbf{r} = 0$ [2]. This leads to

$$a_{p;n,m} = \Delta^2 DFT^{-1} \left[DFT[g_{n,m}] DFT[\chi_{n,m}^{(p)} d_{p;n,m}] \right],\ p = 1, 2, 3. \quad (7)$$

in which

$$\chi_{n,m}^{(1)} = \frac{1}{2}(\chi((n-1)\Delta, m\Delta) + \chi(n\Delta, m\Delta)), \quad \chi_{n,m}^{(2)} = \frac{1}{2}(\chi(n\Delta, (m-1)\Delta) + \chi(n\Delta, m\Delta)), \quad (8a)$$

$$\chi_{n,m}^{(3)} = \frac{1}{4}(\chi((n-1)\Delta, (m-1)\Delta) + \chi((n-1)\Delta, m\Delta) + \chi(n\Delta x, (m-1)\Delta x) + \chi(n\Delta x, m\Delta x)). \quad (8b)$$

The system of equations (3) and (7) is iteratively solved for the unknowns $d_{p;n,m}$ using a BiCGS-scheme [3].

III. Numerical and experimental results

A. Comparison to analytic solutions for TM and TE polarizations

In the simulations with our 2.5D BiCGS-FFT forward solver the initial estimate for d_p ($p = 1, 2, 3$) is chosen zero and the BiCGS iterations are stopped when the relative error drops below 10^{-8}. The object is a dielectric cylinder with relative permittivity $\epsilon_r = 2$ and with a radius equal to one wavelength ($\lambda_0 = 1$ mm, $f = 300$ GHz). We first consider TM polarization. The incident field $E^i(\mathbf{r}) = E_3^i(\mathbf{r})$ is a line source at a distance of $10\lambda_0$ from the cylinder. The scattered fields $E_3^s(\mathbf{r})$ are calculated for 256 points on a circle with a radius of $10\lambda_0$. A good agreement with the analytical solutions is observed in Fig. 1. Fig. 2 shows the normalized root mean square error (NRMSE) for five different discretizations: 8, 10, 20, 100 and 500 cells per λ_0. The error decreases as $O(\Delta)$. Next we consider TE polarization. The incident field $E^i(\mathbf{r}) = E_1^i(\mathbf{r})$ is a plane wave propagating in the y-direction, which is polarized along the x-direction. The scattered fields $E_1^s(\mathbf{r})$ are calculated in the same points as before. In Fig. 3, we observe again a good agreement with the analytical solutions. Fig. 4 shows the NRMSE for the same discretizations as in the TM case.

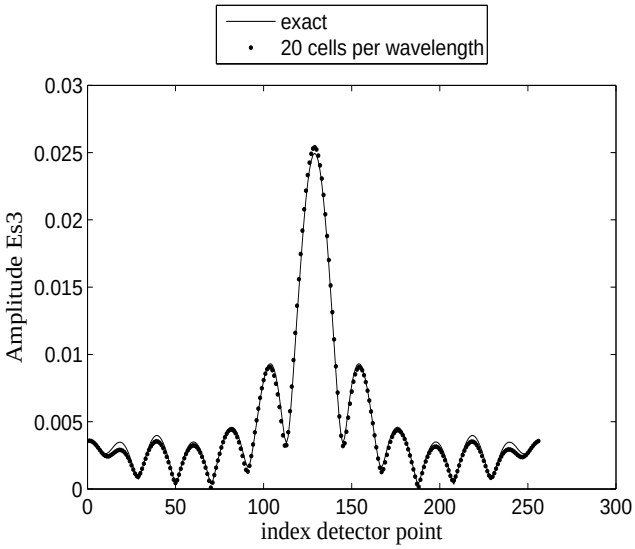

Fig. 1. Amplitude of scattered field for TM simulation

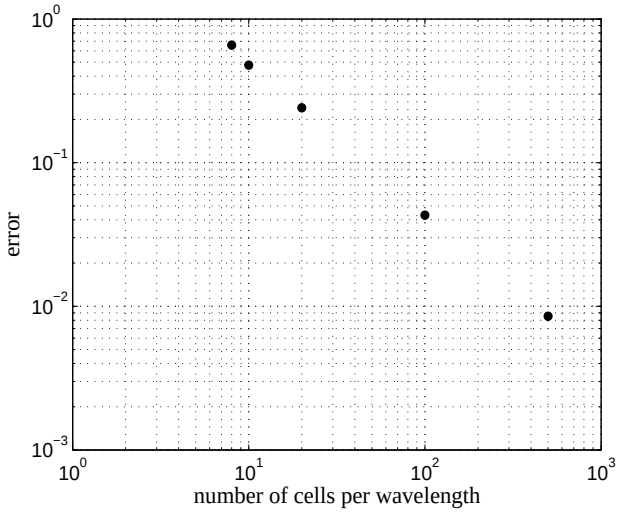

Fig. 2. Error in TM simulation

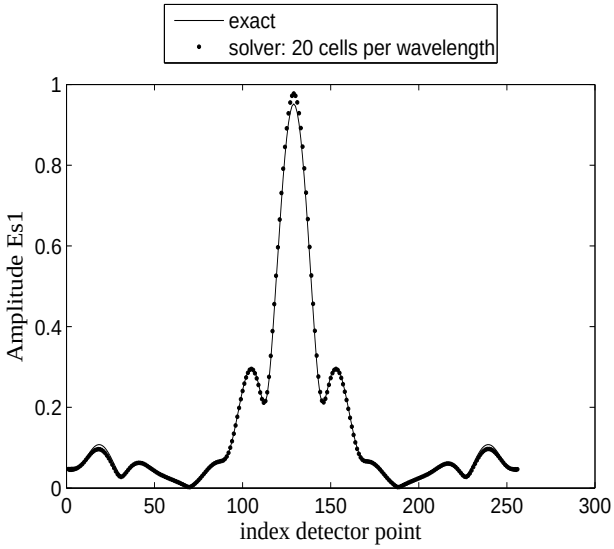

Fig. 3. Amplitude of scattered field for TE simulation

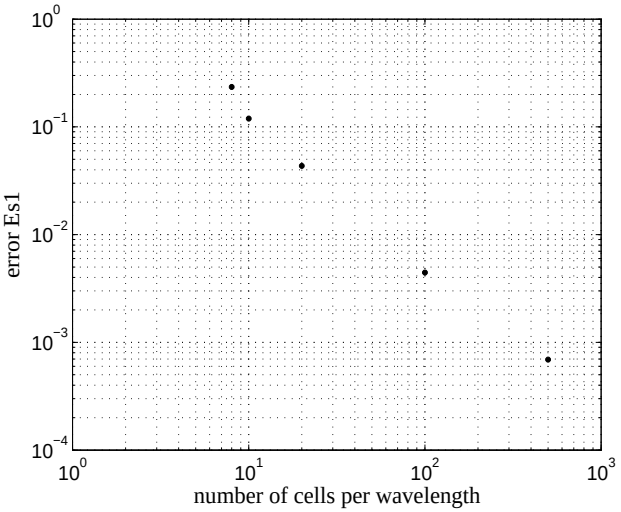

Fig. 4. Error in TE simulation

B. Comparison to measurements for TE-polarization

Fig. 5 represents the measurement setup used to validate our model. A W-band BWO (Backward Wave Oscillator) emits a 94GHz wave which is modulated by a lock-in amplifier with a 20 kHz signal and which is focused into a gaussian beam. The object is positioned along the beam axis to scatter the field. At the detecting side, an open WR10 waveguide probe is used as the receiving antenna. To detect the received signal power, a W-band planar detector with a sensitivity of 550 mV/mW is applied. Its output voltage is fed back into the lock-in amplifier. A 30dB Faraday isolator is placed between the probe and the detector to eliminate the reflection from the planar detector side. The probe, isolator and detector are mounted together on a computer-controlled sled, which is able to move both parallel and perpendicular to the beam axis in a horizontal plane.
The object is a metal cylinder with a diameter of 37.74 mm (which is about $11.5\lambda_0$, $f = 94$ GHz). In our model we choose $\epsilon_r' = 1$ and $\epsilon_r'' = 100$, which corresponds to $\sigma = 523$. No higher values for ϵ_r'' are chosen because the convergence of the BiCGS algorithm significantly slows down. The object is discretized using 10 cells per λ_0, yielding in a grid size of 256x256 cells. The incident field is a gaussian beam which illuminates the object completely. The distance between the source and the object is 45 cm. The total field amplitude is measured on a line of length 8 cm at a distance of 22.5 cm away from the center of the cylinder in 81 points, spaced 1 mm. Fig. 6 shows a comparison of a simulation with a measurement. There is a good agreement in the center of the line. At the edges the difference is propably due to the low value chosen for $\epsilon_r'' = 100$ in our model.

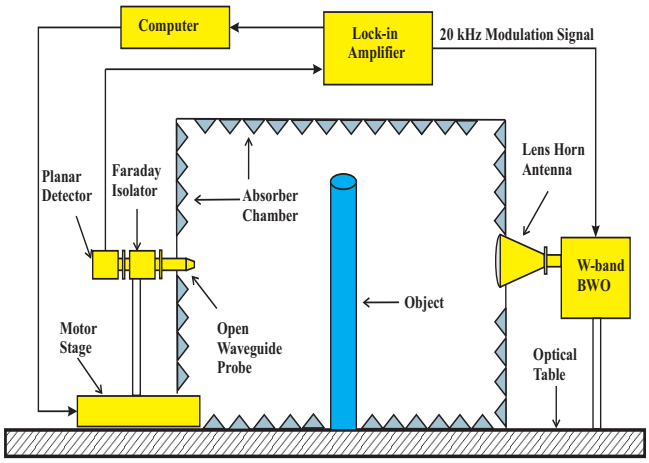

Fig. 5. Schematic diagram of scattering measurement setup

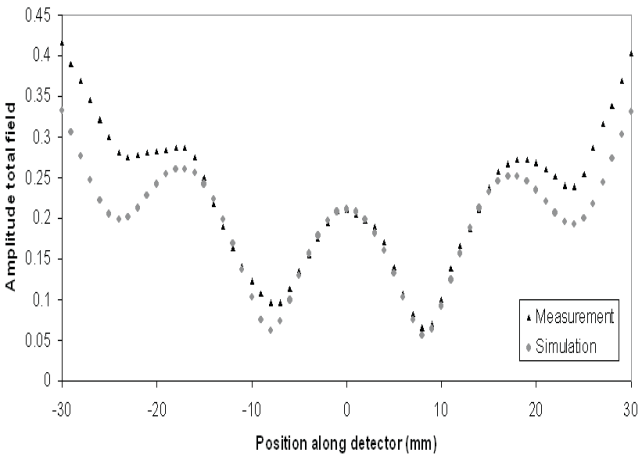

Fig. 6. Amplitude of total field: gaussian beam

IV. Conclusions

A weak formulation of the BiCGS-FFT method for dielectric scatterers is presented. The simulated field curves are in very good agreement with the analytical solutions for TM and TE polarizations. The convolution structure in the vector potential allows the application of FFT's, yielding a fast and efficient method for solving scattering problems. A first comparison to measurements indicates that PEC materials are demanding test objects. In the future, we will also do measurements on various dielectric objects. Moreover, measurements will be done at the VUB with a millimeter wave vector network analyzer so that amplitude *and* phase can be measured and compared to simulations.

References

[1] P. Zwamborn and P. M. van den Berg, "A Weak Form of the Conjugate Gradient FFT Method for Two-Dimensional TE Scattering Problems," *IEEE Trans. on Microwave Theory and Techniques*, vol. 39(6), pp. 953-960, June 1991.

[2] J. H. Richmond, "Scattering by a dielectric cylinder of arbitrary cross section," *IEEE Trans. on Antennas and Propagation*, vol. AP-13, pp. 334-341, May 1965.

[3] X. M. Xu, Q. H. Liu and Z. Q. Zhang, "The stabilized biconjugate gradient fast Fourier transform method for electromagnetic scattering," *J. Appl. Computat Electromag. Soc.*, vol. 17(1), pp. 97-103, March 2002.

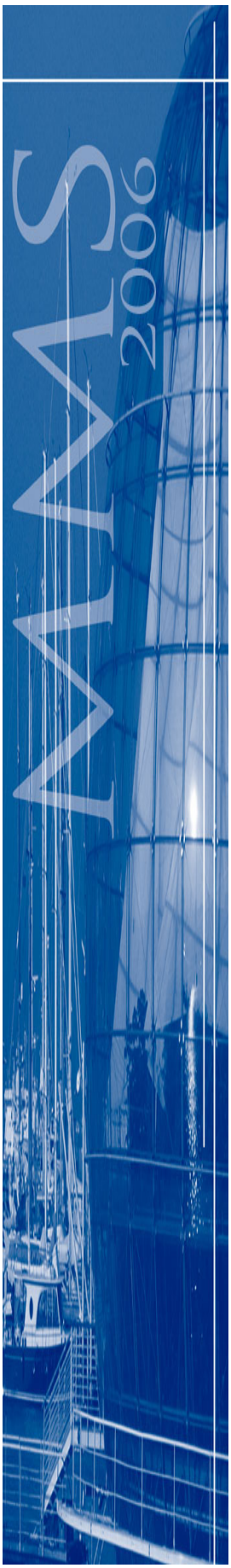

MEDITERRANEAN MICROWAVE SYMPOSIUM 2006

September 19-21, 2006
Starhotel President
Genova, Italy

Conference Proceedings

www.elettromagnetismo.it/conf/MMS2006